Three-dimensional particle simulation of heavy-ion fusion beams*

Alex Friedman† and David P. Grote
Lawrence Livermore National Laboratory, University of California, Livermore, California 94550

Irving Haber
United States Naval Research Laboratory, Washington D.C. 20375

(Received 12 November 1991; accepted 18 February 1992)

The beams in a heavy-ion-beam-driven inertial fusion (HIF) accelerator are collisionless, nonneutral plasmas, confined by applied magnetic and electric fields. These space-charge-dominated beams must be focused onto small (few mm) spots at the fusion target, and so preservation of a small emittance is crucial. The nonlinear beam self-fields can lead to emittance growth, and so a self-consistent field description is needed. To this end, a multidimensional particle simulation code, WARP [Friedman *et al.*, Part. Accel. **37-38**, 131 (1992)], has been developed and is being used to study the transport of HIF beams. The code's three-dimensional (3-D) package combines features of an accelerator code and a particle-in-cell plasma simulation. Novel techniques allow it to follow beams through many accelerator elements over long distances and around bends. This paper first outlines the algorithms employed in WARP. A number of applications and corresponding results are then presented. These applications include studies of: beam drift-compression in a misaligned lattice of quadrupole focusing magnets; beam equilibria, and the approach to equilibrium; and the MBE-4 experiment [*AIP Conference Proceedings 152* (AIP, New York, 1986), p. 145] recently concluded at Lawrence Berkeley Laboratory (LBL). Finally, 3-D simulations of bent-beam dynamics relevant to the planned Induction Linac Systems Experiments (ILSE) [Fessenden, Nucl. Instrum. Methods Plasma Res. A **278**, 13 (1989)] at LBL are described. Axially cold beams are observed to exhibit little or no root-mean-square emittance growth at midpulse in transiting a (sharp) bend. Axially hot beams, in contrast, do exhibit some emittance growth.

I. INTRODUCTION

Heavy-ion particle accelerators are attractive candidates as drivers for inertial fusion energy applications.[1] Among the virtues of existing accelerators used for high-energy physics research are reliability (typically greater than 90%), efficiency (15% to 35%), long life expectancy (tens of years), and compatibility with a high pulse repetition rate. Furthermore, good indirect-drive beam-target coupling is expected, with high x-ray conversion efficiency, low preheat, and absence of deleterious collective instabilities. In addition, the HIBALL-II study has shown that the final optic (a magnetic lens) can be made "survivable" with respect to neutron damage.[2] However, in a fusion driver, it is necessary to transport a much larger current than has been achieved in existing ion accelerators, and the physics of high-current beams is considerably more complicated than that of the low-current beams in conventional ion accelerators. This is especially the case for the recirculating induction accelerator being studied at Lawrence Livermore National Laboratory (LLNL) as a lower-cost alternative to a linear driver for fusion energy.[3]

The beams in a high-current accelerator are collisionless, nonneutral plasmas, confined by applied magnetic and electric fields. These space-charge-dominated beams must be focused onto small (few mm) spots at the fusion target, and so preservation of a small beam emittance is crucial. In contrast with beams in low-current accelerators, the large nonlinear self-fields of space-charge-dominated beams can lead to emittance growth, especially when the beam undergoes many manipulations, which may include: transport around bends (needed to enter the target chamber, or for recirculation); transport through imperfectly aligned focusing elements; nonsteady acceleration; injection into rings; merging; and splitting. Thus a self-consistent field description is needed. Because of the beam's low plasma frequency and short residence time, particle-in-cell (PIC) techniques are particularly well suited to computations for heavy-ion-beam-driven inertial fusion (HIF) applications.[4]

We have developed a multidimensional particle simulation code, WARP, and are using it to study the transport of HIF beams.[5–10] The code's three-dimensional (3-D) package (three spatial dimensions) is known as WARP6 because of its "warped Cartesian" geometry and six-dimensional (6-D) phase space; it combines features of an accelerator code and a PIC plasma simulation. Novel techniques allow it to follow beams, for the first time in 3-D, through many accelerator elements over long distances and around bends. Applications include studies of: (1) the drift-compression current-enhancement process, whereby the beam's tail is imparted a velocity larger than that of its head and the beam allowed to shorten, and especially the effects of quadrupole magnet misalignments on this process; (2) beam equilibria, axial confinement, and the approach to equilibrium; (3) beam emittance growth that

*Paper 8I7, Bull Am. Phys. Soc. **36**, 2455 (1991).

†Invited author.

 0899-8213/92/072203-08$04.00

was observed in the MBE-4 experiment at Lawrence Berkeley Laboratory (LBL) under conditions of aggressive axial compression;[8] and (4) beam transport around bends, specifically, in the planned ILSE experiments at LBL.[11,12] Some of these results are presented here.

II. CODE OVERVIEW

The WARP code consists of: WARP6; WARPRZ,[10] an axisymmetric (five-dimensional phase space) PIC package; ENV, a package that solves an equation describing the beam envelope, which is used to load particles so as to start each PIC run with a "matched" near-equilibrium beam; and facilities for diagnostics, etc. The code uses BASIS,[13] which provides a code development system that facilitates modular construction of programs, and also affords a powerful interactive user interface.

The code's model accelerator "lattice" consists of a fully general set of finite-length (for now, sharp-edged) focusing and bending elements. The electric and magnetic fields of these elements (which have properties such as location, strength, etc., specified by the code's user) are computed in the local laboratory frame algebraically at each particle location at each time step. In combination with the self-fields, these applied fields are used in the Lorentz force law to advance the particle velocity time-step-by-time-step. Each multipole component (azimuthal harmonic, using the accelerator centerline as an axis) of the applied field is handled separately; for flexibility, different multipoles can overlap axially. The lattice can be made periodic, including periodic alignment errors, to simulate a recirculator or storage ring. Alternatively, the lattice can be periodic, but with aperiodic errors, to simulate a repetitive structure. For efficiency, we load a uniform 1-D grid with lattice information (element starts, ends, strengths, etc.) at the beginning of each time step. When advancing the particles, we extract the necessary lattice data from this grid, rather than from the master lists of elements.

In a numerical calculation of particle trajectories (for example, the leapfrog advance that we use), if a particle were to land within a sharp-edged focusing or bending element on four steps while its neighbor did so on only three, they would receive dramatically different impulses. Thus the advance is modified to incorporate "residence corrections" for element forces; these corrections multiply the applied field by the fraction of the velocity advance step spent within the element. This technique allows much bigger computational steps than are otherwise possible.

For efficiency on modern supercomputers, such as the Cray X/MP and Cray 2,[14] the particle advance is vectorized, that is, arranged so that many similar operations can take place in very rapid succession. Deposition of a particle's contribution to the charge density ρ on the computational mesh is also vectorized, but with a short vector of length eight, depositing "simultaneously" into the eight cells overlapped by each particle.

The computational mesh for the self-field, which is assumed electrostatic in the beam frame, moves with the beam and is laid down anew at each time step. To model driver-scale beams (which are mildly relativistic, with speeds up to about $c/3$), we plan to use Lorentz transformations (at least in simple straight systems) to obtain the lab-frame self-**E** and **B** needed to advance the particles. For the present, to model the slower beams of near-term experiments, we use $\mathbf{E}_{self}$ directly to good approximation.

The self-potential ϕ is obtained via vectorized fast Fourier transform (FFT) operations, which assume periodicity in the axial coordinate z but use a Fourier-sine representation in each of the transverse coordinates x and y. These are implemented in such a way as to use negligible scratch space. Self-field boundary conditions are most naturally those of a square metal pipe at the transverse (x,y) edges of the mesh. A round pipe, or other shape independent of z, can be obtained by use of a 2-D (transverse) capacity matrix applied independently to each axial Fourier mode.[9] More general methods that relax the z-independence restriction are under development.

No mesh arrays for the components of **E** are used; instead, values of ϕ are gathered from 32 cells in the neighborhood of each particle, and then differenced to obtain **E** at that particle's location. This saves the space of three 3-D arrays.

Elongated zones (aspect ratios of order 10:1) have been found to work well, provided the axial zone size is less than the beam radius. The time step size Δt is chosen to resolve external field gradients, except at sharp transitions where residence corrections are employed. Accurate trajectories are a necessity. The plasma period is long ($\mathcal{O}$ $100\Delta t$) and well resolved.

III. BENT-BEAM PARTICLE DYNAMICS

We have developed a family of techniques for modeling accelerator bends. These are based upon following a particle's position and velocity in a sequence of Cartesian (laboratory) frames. This "warped" coordinate system is natural for the description of accelerators that include bends.

A method in this family can be implemented in such a way as to compute the necessary coordinate transformations exactly. We have tested that method in a single-particle code, but have not implemented it in WARP; however, a relativistic generalization of it has been successfully applied in the electron accelerator code ELBA.[15] In that method, a particle is advanced using, e.g., a leapfrog advance in the coordinate system associated with the particle's location at the beginning of the step. Then, the particle's position and velocity are algebraically transformed into the rotated inertial coordinate system associated with its location at the end of the step. The scheme conserves phase-space area identically, and implies no large-aspect-ratio (gentle bend) expansion. Its numerical properties are those of the underlying difference scheme. The exact method has a non-negligible operation count, but is quite usable. Here, we describe a simpler approximate method now used in WARP6, which is both faster and sufficiently accurate for present purposes.

In our coordinate system, the radius of curvature of the reference orbit (usually the vessel centerline) is r_*.

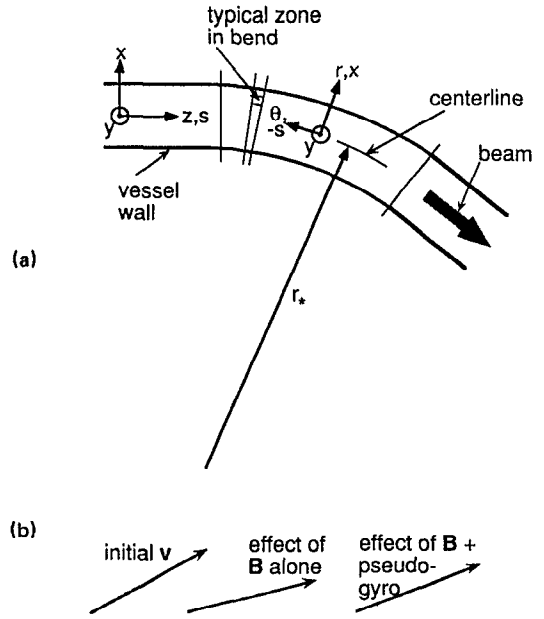

FIG. 1. Geometry of the bent-beam algorithm. (a) Simulation domain and coordinate system; (b) effect of folding the pseudogyromotion associated with coordinate rotation into the bending field.

Time is the independent variable for particle orbits. The conventional independent variable s of many accelerator codes is a dependent variable for orbits in WARP, as are the transverse coordinates x,y. In the straight sections, $s \equiv z$, while in the bends, $s \equiv -r_* \theta$. The "radial" coordinate in WARP is $x \equiv r - r_*$; the unit vectors $\hat{x}$ and $\hat{s}$ evolve as a particle moves, and are different for each particle. This geometry is depicted in Fig. 1(a). The axial speed in a bend is $v_z = -r\dot{\theta}$. The axial position (projection onto the centerline) is advanced in time using

$$\frac{ds}{dt} = -r_* \dot{\theta} = \left(\frac{r_*}{r}\right) v_z. \tag{1}$$

The velocity vector of a particle rotates because of the rotation of the coordinate axes. Due to coordinate transformation alone, the rate of change of the velocity angle is

$$\frac{d}{dt} \arctan\left(\frac{v_x}{v_z}\right) = -\dot{\theta} = \frac{v_z}{r_* + x}. \tag{2}$$

Implementation of the simplified method in WARP was straightforward. We needed only to augment the physical dipole (bending) field with a "pseudogyrofrequency":

$$B_{y,\text{dipole}} \Leftarrow B_{y,\text{dipole}} - \frac{m}{q} \frac{v_z}{r_* + x}, \tag{3}$$

where m is the particle mass and q its charge. This folds the necessary back rotation into existing coding; residence corrections must be used on bend entry or exit. The net effect is depicted in Fig. 1(b). We must also advance the axial position s using Eq. (1) with residence correction. The algorithm is inexact because v_z and x are nonconstant over a time step.

We solve Poisson's equation in "warped" coordinates using a simple, rapid iteration. Poisson's equation (using $h \equiv 1/r_*$) is[16]

$$\frac{1}{1+hx}\frac{\partial}{\partial x}\left((1+hx)\frac{\partial \phi}{\partial x}\right) + \frac{\partial^2 \phi}{\partial y^2} + \frac{1}{1+hx}\frac{\partial}{\partial s}\left(\frac{1}{1+hx}\frac{\partial \phi}{\partial s}\right) = -4\pi\rho. \tag{4}$$

We differentiate the products, and move all terms except the dominant Cartesian-like second-derivative terms to the right member (the source term). The latest ϕ values are used to explicitly compute these smaller non-Cartesian terms. At each iteration, a 3-D FFT inverts the Cartesian ∇^2 operator. The iteration converges rapidly to relative changes in ϕ of 10^{-6} in two or three passes; this corresponds to a typical relative error in the Poisson equation of $\sim 10^{-8}$.

In a bend, axial zone spacing varies with x. We thus use $\rho = \rho_c r_*/r$, where ρ_c is collected from the particles as for a straight system. The axial field is $E_z = -(r_*/r) \times \partial\phi/\partial s$.

IV. EMITTANCE MEASURE

Emittance is a measure of phase space occupied by the beam. By the Vlasov equation (a good approximation for HIF beams), the 6-D phase-space volume of a collisionless beam is conserved. However, evolution of the 6-D particle distribution away from a smooth ellipsoid can lead to tangling of the distribution and entrainment of empty phase space in an irreversible manner, rendering the underlying microscopic phase-space volume conservation irrelevant to beam focusability.

Usually, one is concerned with transverse emittance and examines the phase-space occupancy of the (x,x') and (y,y') planes separately; here $x' \equiv v_x/v_z$ is the slope of a trajectory's projection into the horizontal (x,z) plane, $y' \equiv v_y/v_z$ that into the vertical (y,z) plane. The maximum allowable transverse emittance is set by the need to hit the target from a standoff distance equal to the reactor chamber radius, using a final optic of reasonable size.

In WARP, we use a root-mean-square (rms) based measure ϵ_x, which is referred to as an effective emittance:

$$\epsilon_x \equiv 4\sqrt{\langle (x-\langle x\rangle)^2\rangle \langle (x'-\langle x'\rangle)^2\rangle - \langle (x-\langle x\rangle)(x'-\langle x'\rangle)\rangle^2}. \tag{5}$$

This gives the area, in, e.g., π-m-rad or π-mm-mrad, of a uniformly filled ellipse. (The "π" is often explicitly included in the units.) Here, angle brackets denote an average over particles.

Considerable care has gone into the implementation of the emittance measure in WARP. At any one time, the particles are all at different z's. We first map (using the present and previous velocity) each particle's transverse position and velocity into the values they would have at the nearest two points of a uniformly spaced set of axial locations. This prevents rotation of the phase ellipse with z from acting as a spurious contribution to the emittance; if a straightforward moment were taken over particles with a range of z's, the emittance would appear unduly large. Then, the contribution of a particle to each point of the set is weighted by its proximity to that point.

Under ideal circumstances, i.e., perfectly linear focusing element fields and self-forces [the latter result from a uniformly filled ellipse in (x,y) and require the absence of collective instability], ϵ_x is conserved. Distributions with uniform density include the Kapchinskij–Vladimirskij (K–V)[17] and the so-called semi-Gaussian (Gaussian in velocity, uniform in position) distributions. However, either of these distributions may evolve away from uniform density via instability or lack of equilibrium. Under real circumstances, the emittance will generally grow, either slowly or rapidly. This comes about as a result of higher multipole fields in focusing and accelerating elements, and of nonlinear space charge in high-current beams.

Even in the absence of severe distortion of the phase ellipse, our rms-based emittance measure need not be conserved. It can, in fact, even decrease with time as the beam distribution evolves. Although the rms emittance measure does tend to give heavy weight to so-called outlier particles, we nonetheless generally find it an adequate measure for the not-overly-distorted distributions that are acceptable in practice.

Only those phase-space structures that cannot be unwound downstream by corrective optics must be considered as contributing to the emittance. Other, less readily computed, emittance measures might better take this fact into account. One alternative measure defines emittance as the area of the smallest phase ellipse that contains 95% of the particles. This ellipse will include contributions from entrained empty space in the emittance, but will not give undue weight to outlier particles since they will not fall in the 95%. We are investigating the practicality of implementing a second measure along these lines.

V. DRIFT COMPRESSION OF AN ILSE-SCALE BEAM IN A MISALIGNED LATTICE

We have considered[7] current amplification in a beam initialized with a 7.5% head-to-tail velocity gradient. The focusing lattice was given random transverse misalignments of the magnetic quadrupole elements. The initial profile assumed a uniform line charge density over the central body of the (1.5 m long, perhaps half that of the planned experiments) beam. The cross section of the initial beam at any axial position is an ellipse, and the initial beam has uniform density everywhere within its confines. A parabolic dependence of the line-charge density upon z is assumed at the beam ends. So that a single (scaled) envelope solution could be used, it was assumed that $\epsilon_x(z) \propto a^2(z)$, where a^2 is the transverse cross-sectional area of the beam. Both K–V and semi-Gaussian beams have been followed through 30 magnets (using 900 computational time steps).

Most of these runs used 54 160 particles and a $64\times64\times128$ spatial mesh. The time-step size corresponded to 2 cm/step. A typical run of this type uses about 40 min of Cray X/MP time, including diagnostics.

Our algorithms do not enforce conservation of total energy; the degree to which it remains constant serves as a measure of code performance. In the runs discussed here, the total energy is typically well conserved; variations in total energy are of order 1% of the fall in kinetic energy over the course of the run.

In reference runs with no misalignment, the emittance at pulse center is observed to remain aproximately constant. With square conducting walls and 1 mm (rms) misalignments, ϵ_x and ϵ_y grow by about 25%; this results from the beam's side-to-side oscillations bringing parts of it closer to the square conducting walls (7 cm from pipe center), where image effects lead to nonlinear fields and cause emittance growth. The growth disappears when the walls are moved out to 9 cm. Details of the misalignment are significant. In typical runs, the centroids in x and y are deflected by different degrees.

VI. BEAM EQUILIBRIA AND THE APPROACH TO EQUILIBRIUM

In order to follow beams over long distances, it is necessary to apply an axial confining force to prevent expansion of the beam ends. Such expansion arises because the axial variation of the line-charge density λ near the beam ends leads to an electrostatic self-field that is approximately proportional to $\partial\lambda/\partial z$. In a driver, as well as in current and near-term experiments, the confinement is obtained by shaping the accelerating pulses as the beam ends pass by. These additional pulse features are referred to as "ears."

In many of our simulations, inwardly directed axial forces that move with the beam are applied continuously at the beam ends; the force applied is the negative of the initial axial self-force, plus an additional smaller term arising from the beam's axial pressure gradient.[9,18] Using this capability, we have followed beams for as long as 175 strong-focusing lattice periods, or over 210 m in 10 500 time steps. In one such test, the beam was given comparable initial axial and transverse temperatures. The emittance at pulse center remained essentially constant over the entire course of the run, showing that nonphysical numerical heating (a common difficulty of particle codes) is well controlled.

The emittance at the beam ends grows by as much as 50%; this is believed to be a physical effect, a consequence of the simple emittance scaling (emittance proportional to current) with which the beam ends were initially loaded.

While convenient, this scaling ansatz does not represent a true equilibrium, which appears to be more nearly like a blunt-edged beam with more tenuous tips that are associated with a larger emittance than was assumed. We plan to run one of these beams for a long enough time to reach an asymptotic state, so that we can study a true equilibrium configuration.

We are also studying equilibration processes[7] that transfer thermal energy between transverse and longitudinal motions. Some beams that are initially colder in z than in x,y are observed in our simulations to heat rapidly in z until T_z is a large fraction of $T_{x,y}$. Previous researchers have noted collective equilibration mechanisms, driven by an anistropic distribution function, in other geometries.[19,20] If $T_{x,y}$ indeed cannot greatly exceed T_z, this would represent a constraint on driver design. For current designs, $T_{x,y}$ is, in general, of order T_z over most of the accelerator, and so such a collective equilibration constraint would be likely to have little if any effect. We will be monitoring the issue as our driver concepts evolve.

VII. MBE-4 EXPERIMENT

Most of the experimental work on HIF accelerator physics is centered at Lawrence Berkeley Laboratory, with smaller efforts at the University of Maryland and LLNL. The single-beam transport experiment[21] showed that strongly space-charge-dominated beams could be transported stably, alleviating earlier fears that this would not be possible. The most recent series of experiments, just completed, used the MBE-4 facility.[22,23] This facility, the first multibeam, current-amplifying ion induction linac, transported and accelerated four beams in tandem, using a single series of accelerating gaps for all four beams. The accelerator was 12–20 times as long as a beam bunch; it was used for longitudinal dynamics and beam control experiments with favorable results, and for studies of transverse emittance evolution under conditions of acceleration and compression.

In the latter experiments, transverse emittance growth appears when strongly space-charge-dominated (transversely cold) beams are subjected to aggressive compression. Our simulations[8] show emittance growth very similar to that seen in the experiment. Such growth results mainly from dodecapole components in the electrostatic focusing field, which is imperfect because the quadrupole conductors are round instead of shaped to provide purely quadrupolar equipotentials. These dodecapole components affect the beam only when it has grown fat as a result of the compression. Particles then sample the regions of the accelerator farther from the axis. The agreement between our simulations and the experimental results is not perfect, however. We believe that this is due to such simplifying assumptions in the code as omission of image charges on quadrupole conductors. We are eliminating these assumptions as code development proceeds.

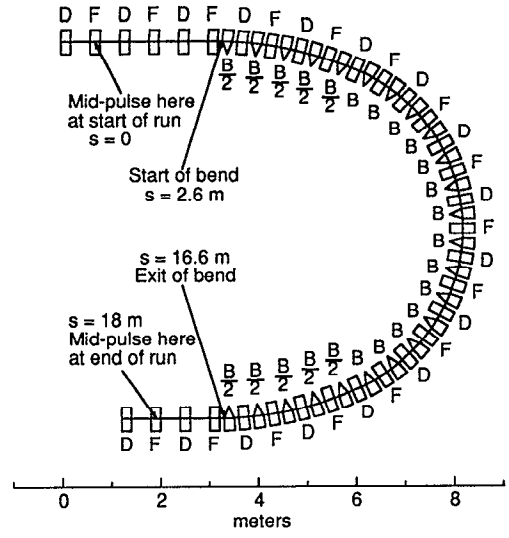

FIG. 2. Model ILSE lattice of example run.

VIII. BENT BEAMS IN AN ILSE LATTICE

A typical lattice of interest for the upcoming ILSE experiments[11,12] is shown in Fig. 2; the F's and D's denote focusing and defocusing quadrupole magnets for the in-plane motion, the B's and $B/2$'s are full- and half-strength

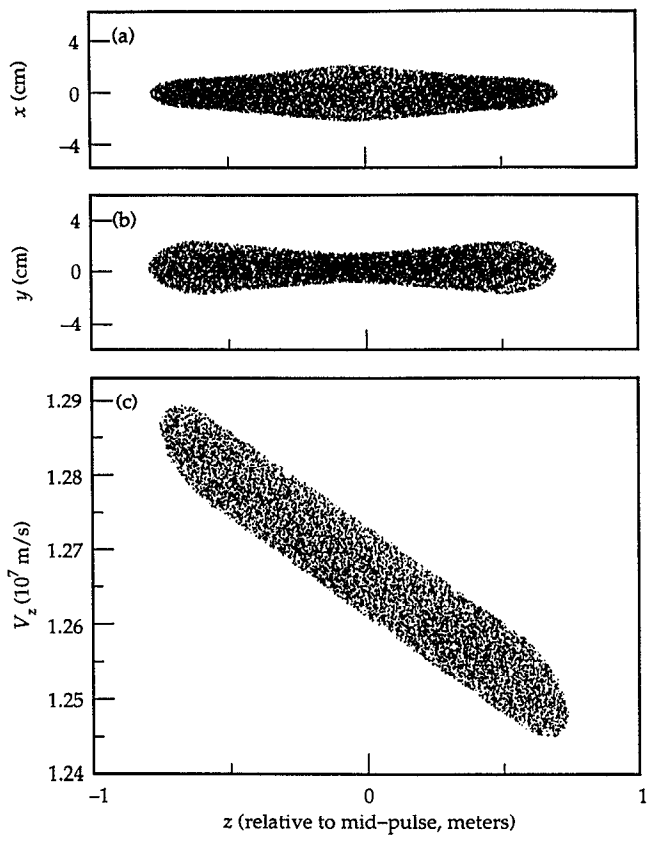

FIG. 3. Snapshot of initial beam for space-charge-dominated bent-beam run (scales are in meters): (a) top view of beam; (b) side view of beam; (c) distribution of axial velocities versus axial position.

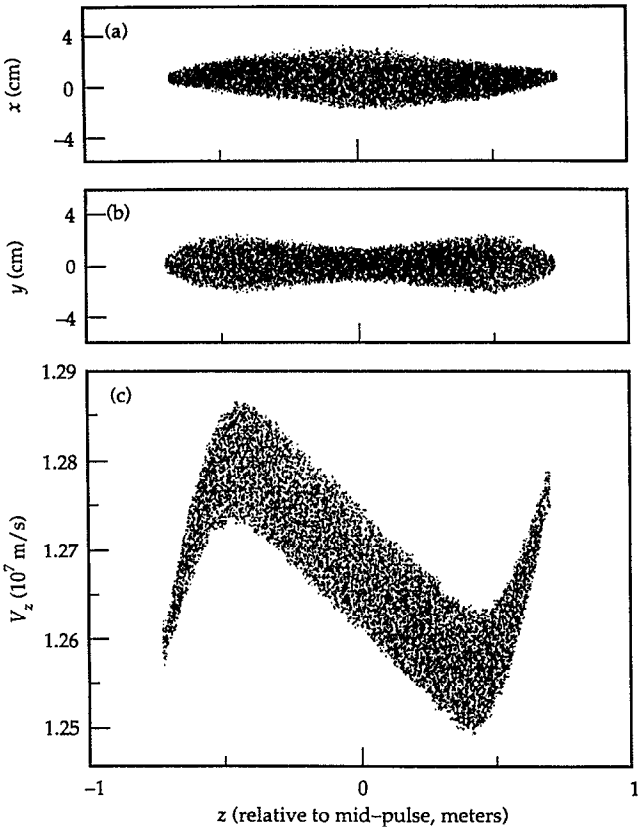

FIG. 4. As in Fig. 3, but after 300 steps (0.474 μsec, 6 m).

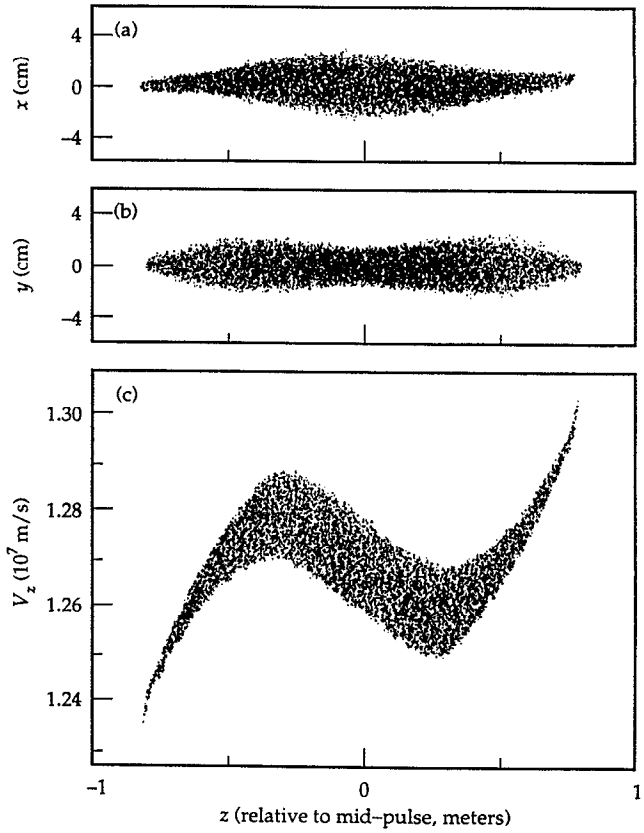

FIG. 5. As in Figs. 3 and 4, but after 600 steps (0.947 μsec, 12 m).

bending magnets. The magnet strengths of this lattice differ very slightly from those of Ref. 12. (This design differs from the most recent ones, which take advantage of a larger experimental site to incorporate a larger radius bend.)

We follow axially cold and axially hot beams with initial head-to-tail velocity gradients around bends. These beams have a ratio of transverse space-charge force to emittance force of about 6:1. The side walls are at ± 6 cm with respect to the accelerator centerline. We assume a singly charged carbon beam, with current 5.2 A and energy 10^7 eV, corresponding to a mean axial ion speed of 1.27×10^7 m/sec. The initial distribution function is semi-Gaussian. This run used a $64\times 64\times 128$ mesh and 54 160 particles. It took approximately 2 h on a Cray X/MP.

For the parameter range considered, simulated axially cold beams exhibit little or no rms emittance growth at midpulse in transiting the very sharp ILSE bend. Furthermore, axially hot ($T_z \sim T_{x,y}$) space-charge-dominated beams do not exhibit emittance growth in straight lattices. Neither do axially hot tenuous beams in bent lattices. Axially hot space-charge-dominated beams in bent lattices, however, do exhibit some emittance growth.[5]

Figure 3 shows the initial particle distribution of an axially hot beam; 3(a) is a top view of the beam, 3(b) is a side view, and 3(c) is a z-v_z projection. (The tail of the beam is at the left in these projections, the head at the right.) Figures 4 and 5 are similar diagnostics taken after the center of the beam has moved 6 m (in 300 time steps) and 12 m (in 600 time steps), respectively. The small, radially inward displacement (toward negative x) of the beam tail is a consequence of the tail's reduced axial velocity, which results from the axial expansion. Figure 6 shows the situation at the end of the run, after the beam has moved 18 m (in 900 time steps).

In Fig. 7, the evolution of the line-charge density is shown via an overlay of snapshots taken at regular intervals; the compression is evident. Figure 8 shows the centroid displacement at various places in the beam. The fact that this displacement returns to approximately zero at each point on the beam, despite their differing axial velocities, is indicative of the achromatic nature of this lattice. This feature is necessary if the beam is to be successfully reinjected into a straight lattice after the bend.

Figure 9 shows a time history of the transverse emittance at midpulse. The hump at midbend in the in-plane emittance is a consequence of the space charge; while it diminishes upon bend exit, some residual emittance growth is present. Furthermore, the emittance that has been generated couples into the out-of-plane (y) motion. The behavior at other points in the beam is very similar, despite the spatially varying axial speed. We believe this emittance growth arises as a result of the dispersion in the bend; particles with differing axial velocities are deflected to varying degrees, leading to a radial smearing of the charge distribution. The nonuniform distribution thus produced

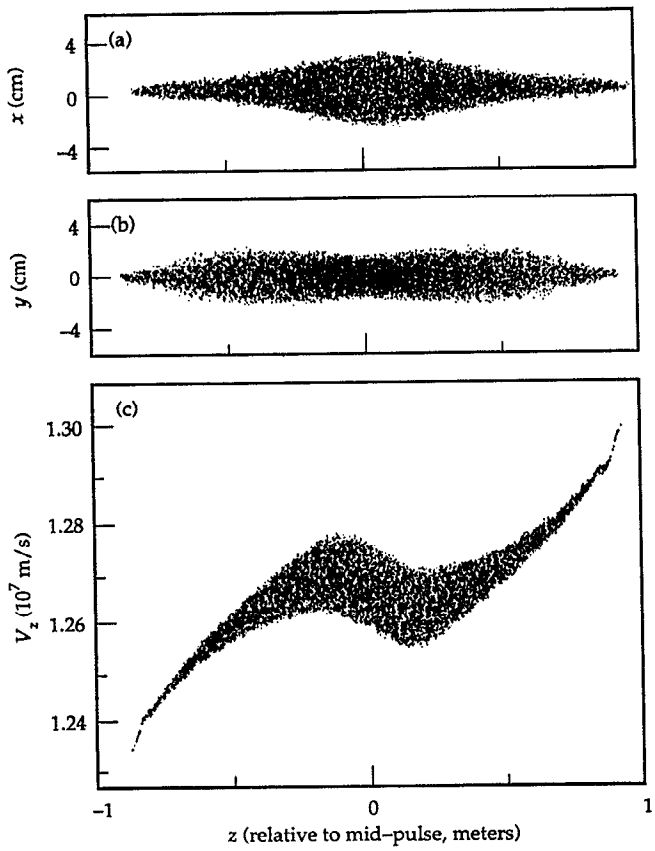

FIG. 6. As in Figs. 3–5, but after 900 steps (1.420 μsec, 18 m).

leads to nonlinear fields that cause the emittance growth. Even though the beam cross sections associated with particles having different longitudinal velocities are partially reunited at the exit to the bend (and so the in-plane emittance $\epsilon_{x-x'}$ diminishes toward the end of the run), genuine 4-D emittance has been created, and, in this, case results in

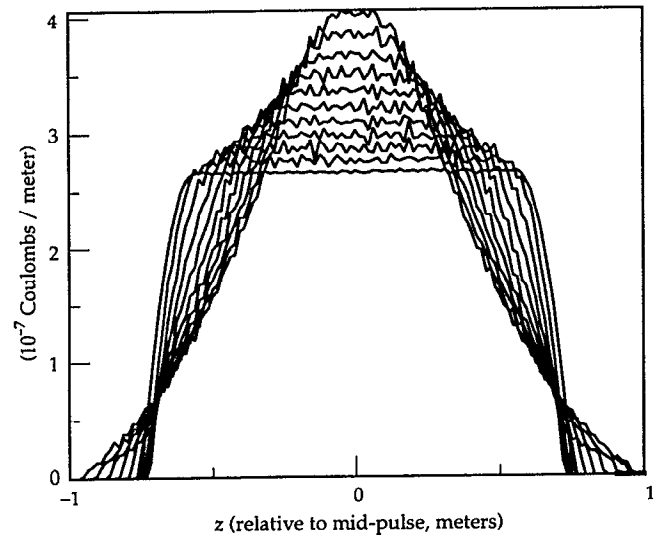

FIG. 7. Line charge density (C/m) versus axial position at various times during the run, showing the pulse compression and density increase.

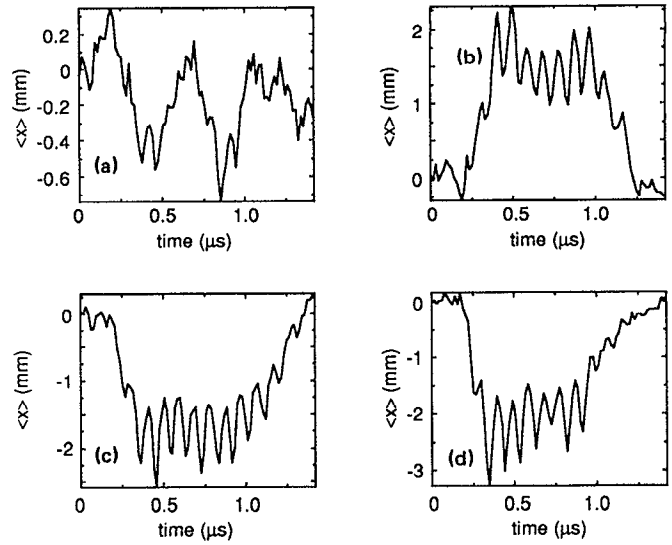

FIG. 8. In-plane displacement (m) of centroid at various places in the beam versus time: (a) at midpulse; (b) 0.3 m toward tail; (c) 0.3 m toward head; (d) 0.4 m toward head.

an increase in $\epsilon_{yy'}$. The mechanism behind this coupling is not yet understood, but such couplings are not uncommon in intense beam dynamics.

In our most recent runs, we have examined a racetrack configuration that might be used in a recirculating induction accelerator.[3] The lattice is similar to the model ILSE lattice studied here, but with two bends separated by straight sections. Axially warm beams in that lattice followed for two-and-one-half laps experience emittance growth similar to that shown here, with a "hump" in $\epsilon_{xx'}$ during each passage through a bend, and a superimposed upward trend even in the straight sections. The out-of-plane emittance grows more nearly monotonically. Axially cold beams exhibit little if any emittance growth in the racetrack. These results will be presented in a future publication.

The ILSE experiments are likely to include the merging of four beamlets into one higher-current beam; this should increase $T_{x,y}$ without increasing T_z, leading to a relatively axially cold beam. Experiments without merging are also likely to be included.

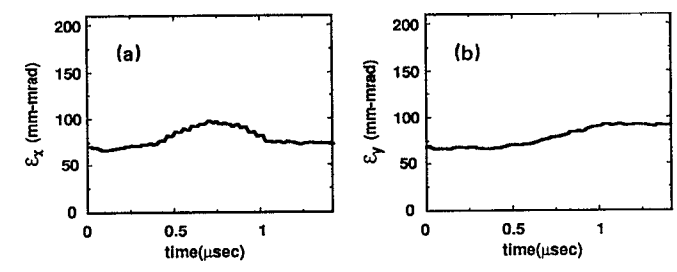

FIG. 9. Midpulse emittance versus time for space-charge-dominated bent-beam run: (a) in-plane (x) emittance; (b) out-of-plane (y) emittance.

IX. PLANS FOR FURTHER RESEARCH

We are investigating methods of modeling electrostatic quadrupole elements from first principles, and plan to refine our MBE-4 simulations. We will also use this capability to model electrostatic confinement in the low-energy stage of ILSE.

Numerous other code improvements, including a magnet fringe field model, a programmed accelerating gap description, and a means of forming beams by injection, are either in progress or are being considered.

We plan to study the effects of intermittently applied confining ears, to learn the limits imposed by beam quality degradation on the allowable interval between their application.

We plan to study the drift-compression process in driver-scale beams and the final-focus process. In the latter regime, the beam is not long and thin, and a 3-D representation may be necessary to capture space-charge effects accurately.

We plan to continue our study of racetrack and ring recirculating accelerator configurations.

We have not discussed here the effort by our collaborators to understand longitudinal beam stability, using the axisymmetric (r,z) model in WARPRZ.[10] A known instability is associated with the impedance of the accelerating modules. While careful design and techniques such as feedforward stabilization should afford suppression of the instability, it is important to be able to model (in a causal, self-consistent way) multidimensional effects such as wave reflection at the bunch ends and radial variations of the interaction between particles and modules. Such effects may be especially significant in the driver-relevant low growth rate regime.

Other natural applications of the (r,z) model include studies of equilibration processes (now in progress), and of the equilibrium axial dependence of the emittance at the beam ends.

ACKNOWLEDGMENTS

The authors are pleased to acknowledge numerous valuable discussions with R. O. Bangerter, D. A. Callahan, A. T. Drobot, A. B. Langdon, J. W-K. Mark, and H. D. Shay, and with other HIF researchers at LBL and LLNL.

This work was performed under the auspices of the U.S. Department of Energy by Lawrence Livermore National Laboratory under Contract No. W-7405-ENG-48, and by the U.S. Naval Research Laboratory under Lawrence Berkeley Laboratory Contract No. DE-AC03-76SF0098.

[1] T. J. Fessenden and A. Friedman, Nucl. Fusion **31**, 1567 (1991).
[2] R. Bock, in *Proceedings of the 1986 International Symposium on Heavy Ion Inertial Fusion*, Washington, D.C., edited by M. Reiser, T. Godlove, and R. O. Bangerter (AIP, New York, 1986), p. 23.
[3] J. J. Barnard, M. A. Newton, L. L. Reginato, W. M. Sharp, H. D. Shay, and S. S. Yu, in *Conference Record of the 1991 IEEE Particle Accelerator Conference*, San Francisco, CA, edited by L. Lizama and J. Chew (IEEE, New York, 1991), p. 2592.
[4] I. Haber, in *Proceedings of the Conference on High-Current, High-Brightness, and High-Duty Factor Ion Injectors*, La Jolla, CA (AIP, New York, 1986), p. 107.
[5] A. Friedman, D. P. Grote, D. A. Callahan, A. B. Langdon, and I. Haber, in Ref. 3, p. 263.
[6] A. Friedman, D. P. Grote, D. A. Callahan, A. B. Langdon, and I. Haber, Part. Accel. **37-38**, 131 (1992).
[7] A. Friedman, R. O. Bangerter, D. A. Callahan, D. P. Grote, A. B. Langdon, and I. Haber, in *Proceedings of the 2nd European Particle Accelerator Conference*, Nice, France (Editions Frontieres, Gif-sur-Yvette, France, 1990), p. 1699.
[8] D. P. Grote, A. Friedman, and I. Haber, Bull. Am. Phys. Soc. **36**, 2415 (1991).
[9] D. P. Grote, A. Friedman, and I. Haber, Part. Accel. **37-38**, 141 (1992).
[10] D. A. Callahan, A. B. Langdon, A. Friedman, D. P. Grote, and I. Haber, Part. Accel. **37-38**, 97 (1992).
[11] T. J. Fessenden, Nucl. Instrum. Methods Plasma Res. A **278**, 13 (1989).
[12] E. P. Lee, Nucl. Instrum. Methods Plasma Res. A **278**, 178 (1989).
[13] P. F. Dubois (private communication).
[14] C. N. Arnold, Comput. Phys. **4**, 514 (1990).
[15] S. Slinker, J. Krall, M. Lampe, and G. Joyce, in Ref. 3, p. 242.
[16] K. L. Brown and R. V. Servranckx, in *Proceedings of the Summer School on the Physics of High Energy Particle Accelerators*, Brookhaven (AIP, New York, 1983), p. 75.
[17] I. M. Kapchinskij and V. V. Vladimirskij, in *Proceedings of the 2nd International Conference on High Energy Accelerators* (CERN, Geneva, 1959), p. 274.
[18] D. Neuffer, IEEE Trans. Nucl. Sci. **NS-26**, 3031 (1979).
[19] I. Hofmann (private communication).
[20] R. A. Jameson, IEEE Trans. Nucl. Sci. **NS-28**, 2409 (1981).
[21] M. G. Tiefenback, Ph.D. thesis, University of California, Berkeley, 1986.
[22] T. J. Fessenden, D. L. Judd, D. Keefe, C. Kim, L. J. Laslett, L. Smith, and A. I. Warwick, in Ref. 2, p. 145.
[23] T. J. Fessenden, in Ref. 3, p. 586.